Slow drag in granular materials under high pressure

Fuping Zhou and Suresh G. Advani

Department of Mechanical Engineering and Center for Composite Materials, University of Delaware, Newark, Delaware 19716, USA

Eric D. Wetzel

Army Research Laboratory, Aberdeen Proving Grounds, Maryland 21005, USA

(Received 22 July 2003; revised manuscript received 4 March 2004; published 16 June 2004)

The resistance offered by a cylindrical rod to creeping cross flow of granular materials under pressure is investigated. The experimental system consists of a confined bed of granular particles, which are compacted under high pressure to consolidate the granular medium. A cylindrical rod is pulled at a constant and slow rate through the granular medium, and the measured pulling resistance is characterized as a drag force. The influence of various parameters such as the velocity of the cylindrical rod, the rod diameter and length, the granular particle size, and the compaction pressure on the required drag force is investigated experimentally. Nondimensional analysis is performed to simplify the relationships between these variables. The results show that the drag force is independent of the drag velocity, is linearly proportional to compaction pressure and rod diameter, and increases with rod length and particle size. Additional compaction experiments show that the effective density of the granular bed increases linearly with pressure, and similar behavior is noted for all particle sizes. These results should prove useful in the development of constitutive equations that can describe the motion of solid objects through compacted granular media under high pressure, such as during ballistic penetration of soils or ceramic armors.

I. INTRODUCTION

The investigation of granular flows is important in several fields, including soil mechanics and the manufacturing of products such as pharmaceuticals, ceramics, and foods. Most of these studies consider fluidized granular flow, which is characterized by low packing density, low pressure, and high velocity [1–4]. These dilute flows are largely governed by the collisions between particles. In contrast, the flow behavior of concentrated granular materials is determined by frictional interactions between particles [5]. A number of experimental [6,7] and numerical [5,8,9] investigations of shear flows of concentrated granular materials have been performed. Ovarlez *et al.* [10] have studied the flow of granular materials pushed through cylindrical tubes. Albert and coworkers [11–15] measured drag force on a cylinder pulled slowly through a granular bed. D'Anna [16] studied the drag resistance of a cylinder immersed in a granular bed, rotating about its long axis. Nasuno *et al.* [17] investigated planar shearing flows of granular beds. In all these experiments, the granular material has at least one free boundary, so that pressure effects are localized and relatively small in magnitude.

The influence of high confinement pressure, however, on concentrated granular flows is not well understood. These flows are particularly relevant to the study of confined ceramic armors. When impacted by a ballistic projectile, stress waves travel rapidly through the ceramic and cause extensive fracturing of the ceramic. As the projectile travels through the pulverized ceramic, the granular material undergoes a combination of compaction, flow, and further fracture [18–20]. Momentum transfer from the projectile to the armor results in very high pressures in the vicinity of the projectile, including within the flowing granular material. If the ceramic is unconstrained, there is little resistance to flow of the frac-tured ceramic, and frictional effects between granules are unimportant [21,22]. However, for confined ceramics, it is evident that intergranular frictional dissipation is critically important and, under certain conditions, may be responsible for absorbing a significant fraction of the projectile's initial kinetic energy [20,23].

The static elastic, yield, and dilatancy properties of granular materials under high pressures have been shown to be strongly dependent on compaction pressure [24–28]. Interrogating the flow properties of granular materials under high pressures has proved more difficult. Flying plate experiments [29] and explosive compression and shearing experiments [30] have provided some limited insight into granular material behavior at very high pressures and shear rates.

In this paper, we perform experiments to directly characterize the behavior of concentrated granular materials under high pressures. In the first set of experiments, the effective density of a packed granular bed is measured as a function of compaction pressure, particle size, and velocity. In the second set of experiments, the drag force for flow past a cylinder is used to characterize the viscouslike properties of a confined and pressurized granular bed as a function of particle size, cylinder geometry, flow velocity, and compaction pressure. A better understanding of such behavior will eventually enable the formulation of new constitutive models or the extension of existing models (e.g., [31–34]), for pressurized flow of confined granular beds.

II. EXPERIMENTS

A. Materials

Three different size white aluminum oxide granules (AG-SCO Corporation, Hasbrouch Heights, NJ) were used for the

TABLE I. Average, maximum, and minimum granule sizes (D_g) for the granular materials investigated, as reported by the manufacturer.

	Average size (μm)	Maximum size (μm)	Minimum size (μm)
Coarse granules	1092	1650	787
Medium granules	483	762	305
Fine granules	165	292	102

experiments. Their average sizes along with the minimum and maximum values are summarized in Table I. A Micromeritics (Norcross, GA) AccuPyc 1330 helium pycnometer was used to measure the densities of the powders, which were found to be 3.94, 3.93, and 3.92 g/cm^3 for the coarse, medium, and fine granule sizes, respectively.

B. Compression experiments

To characterize the compression behavior of alumina oxide under high pressure, the system shown in Fig. 1 was designed and fabricated. Granular material of known mass was placed in the steel containment cylinder and compressed using an Instron mechanical tester. The containment cylinder has an internal diameter (D_c) of 38.1 mm and a maximum chamber height of 38.1 mm. The compression force (F) and cylinder diameter can be used to calculate the applied pressure

$$p = \frac{4F}{\pi D_c^2}, \tag{1}$$

while the effective density (ρ) of the granule bed can be calculated based on the mass of granules (m) and instantaneous height of granular materials (h):

$$\rho = \frac{4m}{\pi D_c^2 h}. \tag{2}$$

Compression experiments were performed on all three particle sizes at cover compression velocities from 0.083 to 0.5 mm/s.

C. Drag force experiments

To characterize the drag force of the cylinder through the granular media under high confinement pressure, the device
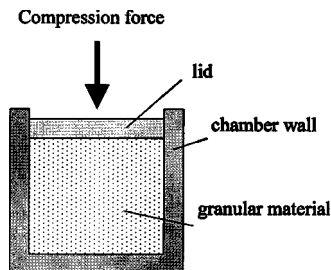

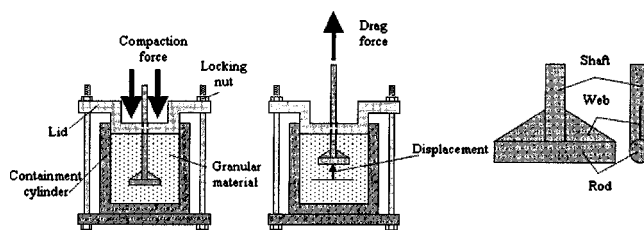FIG. 1. Schematic of the device used for compression experiments.

FIG. 2. Schematic of the device used for drag experiments. (a) Application of compaction pressure. (b) Dragging cylinder through granular bed. (c) Detailed view of the cylinder.

shown in Fig. 2 was designed and fabricated. The containment cylinder has an internal diameter of 101.6 mm and granular materials height of 120 mm. A T-shaped rod is placed inside the containment cylinder, which is then filled with granules and compacted. Two thin, triangular webs are welded at the corners of the T-shaped rod to prevent rod bending during drag. The shaft diameter is equal to the rod diameter. Compaction pressure is applied with the Instron machine and maintained by fixing the volume of the container, via threaded bolts with locking washers through the container lid. An Instron mechanical tester is used to pull the T-shaped rod up through the compacted and confined granular material while monitoring the pulling force and the rod displacement. Drag tests performed using only the shaft, without a T-shaped rod, produced drag force values less than 5% of the comparable T-shaped rod experiments. Therefore the majority of the drag resistance arises from the lower section of the T-shaped rod, which is normal to the flow direction, simulating granular flow past a cylinder.

The method by which the granules are packed into the containment cylinder has a strong influence on the initial void distribution in the packed bed, which in turn can strongly influence the drag behavior [35]. To minimize this effect, for each experiment the cylinder was filled by adding small amounts of powder with compaction applied after each incremental addition of powder. New, untested powder was used for each experiment.

A range of rod diameters (D) (3.175, 4.76, and 6.35 mm), rod lengths (L) (25.4, 38.1, 44.45, and 49.53 mm), and compaction pressures (p) (1.00, 2.00, 3.13, 4.38, and 5.63 MPa) was used with the three different particle sizes. Table II shows the experimental conditions investigated. Experiments performed at different velocities from 0.083 to 0.5 mm/s showed no effect of velocity on drag behavior. The drag force (F) for a given measurement is defined as the average value of the drag force measured between 10 mm and 30 mm of displacement (shown as part II in Fig. 4) and each tabulated value represents the average of at least three experiments (cases with more than three experiments included measurements at various velocities). Note that, for the longest rod (49.53 mm), there is still a gap of 25 mm between the end of the rod and the container wall, so rod-wall interactions should be negligible.

D. Pressure distribution effects

The well-known Janssen effect predicts that frictional interactions between granules and between the granules and

TABLE II. Drag experimental conditions and measured drag force. "S.D." is the percentage standard deviation for the drag force measurements, and "N expt." is the number of experiments performed under those conditions.

Expt.	p(MPa)	$D_g(\mu m)$	D(mm)	L(mm)	F(N)	S.D. (%)	N expt.
1	1.00	165	4.76	44.45	650	2.5	3
2	1.00	483	4.76	44.45	720	4.8	3
3	1.00	1092	4.76	44.45	930	8.7	3
4	2.00	165	4.76	44.45	1150	1.1	3
5	2.00	483	4.76	44.45	1280	7.6	3
6	2.00	1092	4.76	44.45	1740	7.5	3
7	3.13	165	3.175	49.53	1380	3	3
8	3.13	165	4.76	25.4	1400	4.2	3
9	3.13	165	4.76	38.1	1660	4.8	3
10	3.13	165	4.76	44.45	1870	5.1	6
11	3.13	165	4.76	49.53	1920	2.1	3
12	3.13	165	6.35	49.53	2380	2.7	3
13	3.13	483	3.175	49.53	2020	2.3	3
14	3.13	483	4.76	25.4	1560	7.6	3
15	3.13	483	4.76	38.1	2220	10	3
16	3.13	483	4.76	44.45	2270	5.7	6
17	3.13	483	4.76	49.53	2720	3.6	3
18	3.13	483	6.35	49.53	3570	1.8	3
19	3.13	1092	3.175	49.53	2440	10	3
20	3.13	1092	4.76	25.4	1720	7.4	3
21	3.13	1092	4.76	38.1	2430	0.9	3
22	3.13	1092	4.76	44.45	2590	2	6
23	3.13	1092	4.76	49.53	3350	3.3	3
24	3.13	1092	6.35	49.53	3770	2.4	3
25	4.38	165	4.76	44.45	2570	4.3	6
26	4.38	483	4.76	44.45	2950	4.1	6
27	4.38	1092	4.76	44.45	3580	3.9	6
28	5.63	165	4.76	44.45	3240	2.4	6
29	5.63	483	4.76	44.45	3990	4.8	6
30	5.63	1092	4.76	44.45	4090	2.9	6

walls of their container alter the pressure distribution within a dense granular bed. For a closed cylinder with a fixed pressure p_0 on the upper surface, the pressure is expected to decay according to [36]

$$p(y) = p_0 e^{-4y\mu k/D_c}, \qquad (3)$$

where y is the distance from the lid, μ is the wall frictional coefficient, and k is known as Janssen's constant. We can reasonably assume $\mu = 0.5$ and $k = 0.4$. For the compression experiments, the pressure at the bottom of the cylinder ($y/D_c = 1.18$) is approximately 39% of the applied pressure value. Therefore, although we report applied pressure values (p_0), the true average pressure within the bulk of the granular
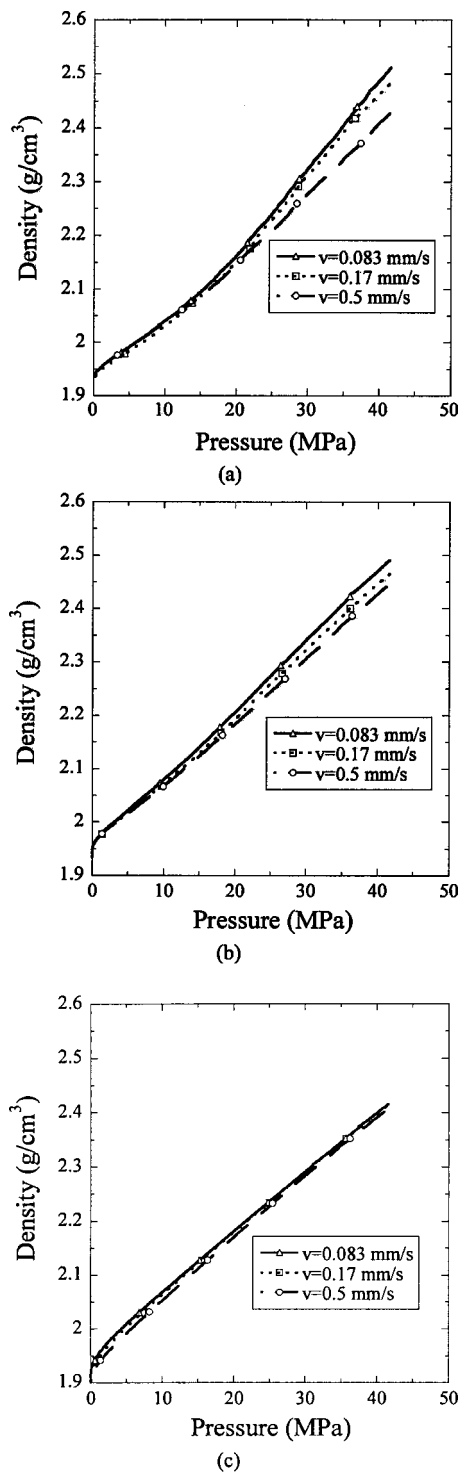

FIG. 3. Compression behavior at various velocities for (a) 1092 μm, (b) 483 μm, and (c) 165 μm granules.

material could be less. For the drag experiments, all experiments are performed from $y/D_c = 1.02$ to $y/D_c = 0.82$ or from a pressure of 44% to 52% of the applied pressure value. The true pressure experienced by the rod could therefore be slightly less than the applied value. However, we know that the pressure changes by only 8% during the course of the experiment, so the constant pressure assumption should be reasonably accurate.
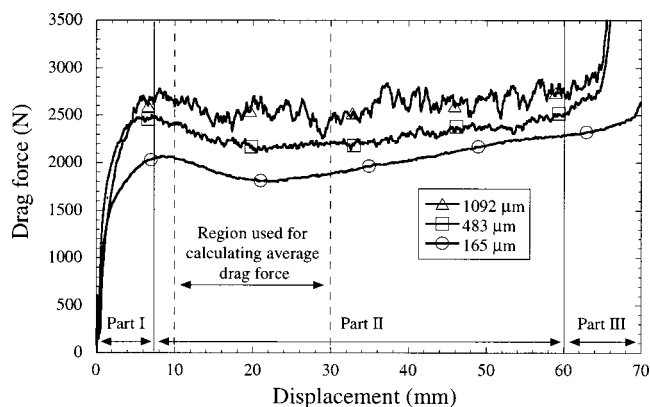
FIG. 4. Generalized behavior during drag experiments, including compaction (part I), steady drag (part II), and cylinder approaching top cover (part III). Parameters for this experiment were $p=3.13$ MPa, $D=4.76$ mm, and $L=44.45$ mm.

III. RESULTS

A. Compression experiments

Figures 3(a)–3(c) show the results of the compression experiments for different particles sizes and compression velocities. In general, density increases approximately linearly with pressure, although within the range of pressures investigated it does not approach the limiting density of the particles themselves (3.9 g/cm^3). For the coarse (1092 μm) particles, increasing velocity decreases the effective density of the granular bed for a given pressure, likely indicating a limiting time scale for reorganization of the grains. For this grain size, slower velocities also produce a more linear dependence of density on applied pressure. For medium (483 μm) particles, the velocity effect is less significant, while little velocity effect is noted for the fine (165 μm) particles.

B. Drag force experiments

Figure 4 shows the general drag behavior observed for these experiments. During the first stage of the experiment (part I), the drag force increases relatively quickly to a peak value. This stage is likely dominated by compression and local reorganization of the granular bed. During the second stage of the experiment (part II), the drag force first decreases slightly and then increases gradually. The initial decrease in the drag force during this stage could be described as a yielding behavior. The subsequent slow growth in the drag force could be due to the rise in pressure associated with the Janssen effect (Sec. II D), or could be caused by accumulated damage, compaction, or particle stagnation in front of the cylinder. However, the total variation in the drag force during this stage is relatively small and is likely indicative of steady, well-developed granular flow past the cylinder. During the final stage (part III), the web of the T-shaped rod approaches the lid of the containment cylinder, and the drag force rapidly increases.

Figure 4 also shows the region chosen for calculating average drag values (10–30 mm). This choice is somewhat
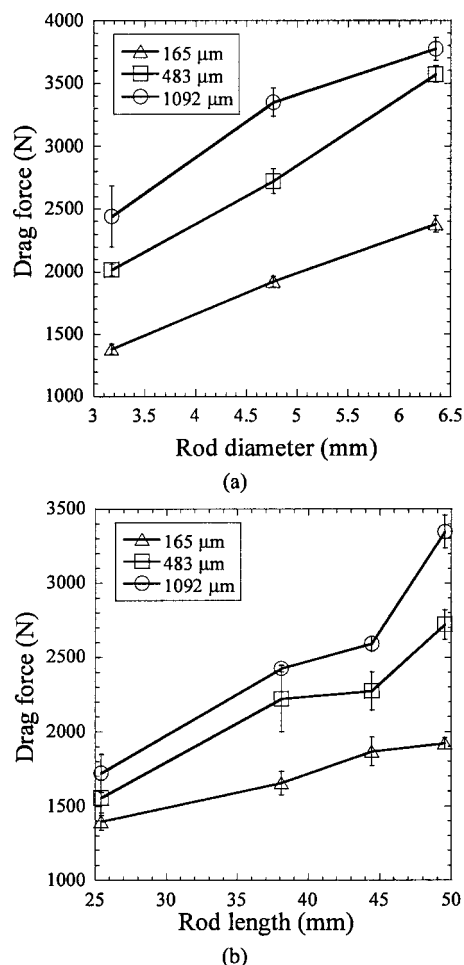

(a)

(b)

FIG. 5. The effect of (a) rod diameter and (b) rod length on drag force, for different particle sizes. All experiments are at $p=3.13$ MPa. For the experiments in (a), $L=49.53$ mm. For the experiments in (b), $D=4.76$ mm.

arbitrary and attempts to capture a typical steady drag force value. Table II shows the average steady drag values measured for each of the experiments. Note that the experiments were very repeatable, with an average standard deviation of 4% and a maximum standard deviation of 10%. Measurements of peak drag force (i.e., at the yield point) produced trends comparable to the average drag force values.

Figures 5(a) and 5(b) show the effect of rod diameter and length on the drag force. For all particle sizes, the drag force increases almost linearly with rod diameter. The drag force also increases with rod length, although the behavior is not clearly linear. Note that the shortest rod length (25.4 mm) is only about 5 times larger than the shaft diameter (4.76 mm), so that end effects and secondary flow perturbations due to the shaft may become significant.

Figure 6 shows the drag force as a function of compaction pressure. For all particle sizes, the drag force increases roughly linearly with pressure.

Figure 7 shows the effect of particle size on the drag force. Larger particles result in more drag force, although a linear dependence is observed only at the lowest pressure. Figure 4 shows the drag force versus displacement for dif-
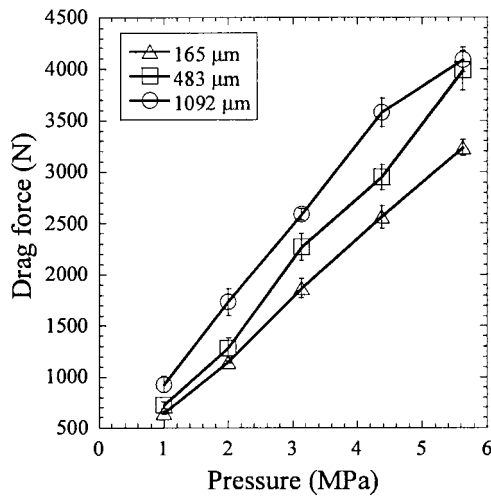
FIG. 6. The effect of pressure on drag force, for different particle sizes. All experiments are for $D=4.76$ mm and $L=44.45$ mm.

ferent particle sizes. Note that the smoothness of the drag force curve increases significantly as particle size is reduced. Also note that during part II the drag force is most steady for the coarse particles, while the finer particles show a more distinct yielding followed by slow growth in the drag force.

Figures 8(a)–8(c) show micrographs of the granules, imaged using a microscope (Leitz Metallux), before and after the drag experiments. In all cases a large fraction of smaller particles are evident after the drag experiment, indicating that significant granule fracture is occurring during the experiment.

IV. DISCUSSION

In order to generalize our understanding of drag flow in pressurized granular materials, we can analyze the results in terms of nondimensional parameters. Figure 9(a) shows the normalized drag force $F/(pDL)$ as a function of granule size. This normalization reduces all of the drag force values to the
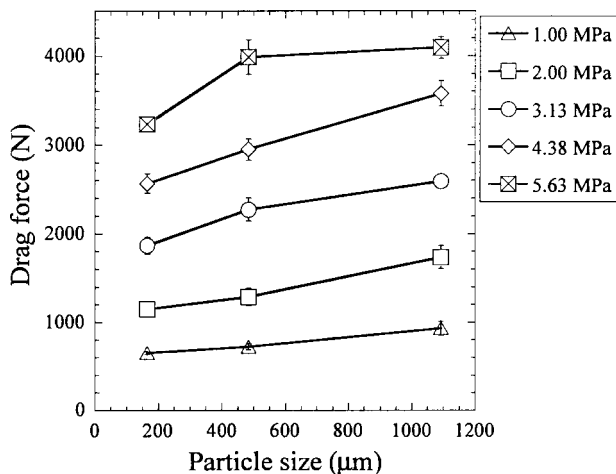

FIG. 7. The effect of particle size on drag force, for different compaction pressures. All experiments are for $D=4.76$ mm and $L=44.45$ mm.
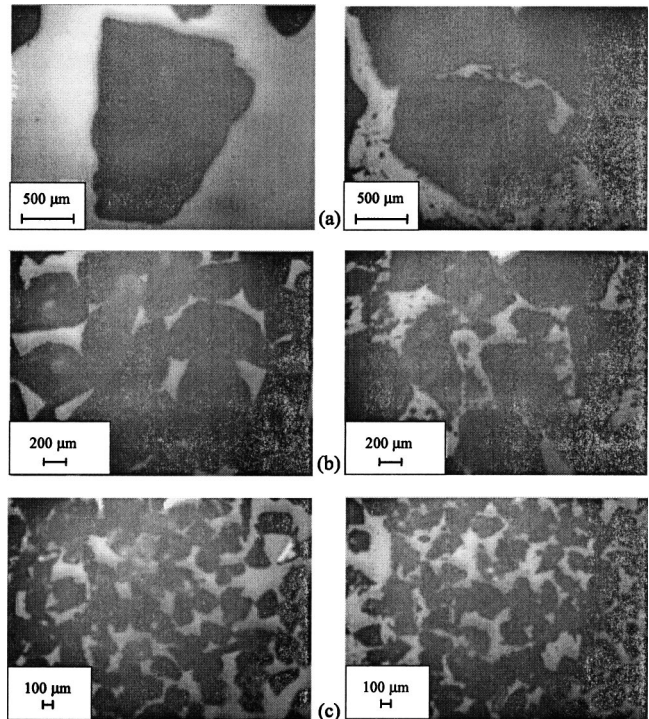

FIG. 8. Micrographs of (a) 1092 μm, (b) 483 μm, and (c) 165 μm particles before (left) and after (right) drag experiments. All micrographs are for $p=5.63$ MPa, $D=4.76$ mm, and $L=44.45$ mm.

order of unity, suggesting that the drag force is largely determined by the pressure drag associated with some areal measure of the cylinder. In fact, the precise numerical values of the scaled force are remarkably close to π, perhaps indicating that scaling the drag force by the surface area of the cylinder may be most appropriate.

Figure 9(a) also shows that the normalized drag force increases with granule size. Figures 9(b) and 9(c) show that the data can be further linearized by presenting the normalized drag force as a function of the logarithm of the geometric ratios D/D_g or $LD/(D_g^2)$. These results, respectively, suggest that pressurized drag flow could be characterized in terms of the cylinder-to-particle size ratio or surface area ratio. Note that linearization of the data and superposition of different pressure results are most successful for fine granules.

Albert *et al.* [11], studying drag on a cylinder pulled through an unconfined granular bed, found that the drag force is linearly dependent on the cylinder diameter, quadratically dependent on the depth of the insertion (cylinder length), and independent of the velocity and granular size. The drag forces for these experiments are also only 1–10 N in magnitude. Our results for confined, pressurized granular materials show that the drag force scales approximately linearly with cylinder diameter, increases with cylinder length, and is strongly dependent on granular size. Pressurization and confinement also obviously lead to dramatic increases in the drag force magnitude, as our measured values range from 1000 to 5000 N for cylinder geometries comparable to those of Albert *et al.*

The increase in drag force with increasing granule size is surprising, since smaller granules are expected to have a
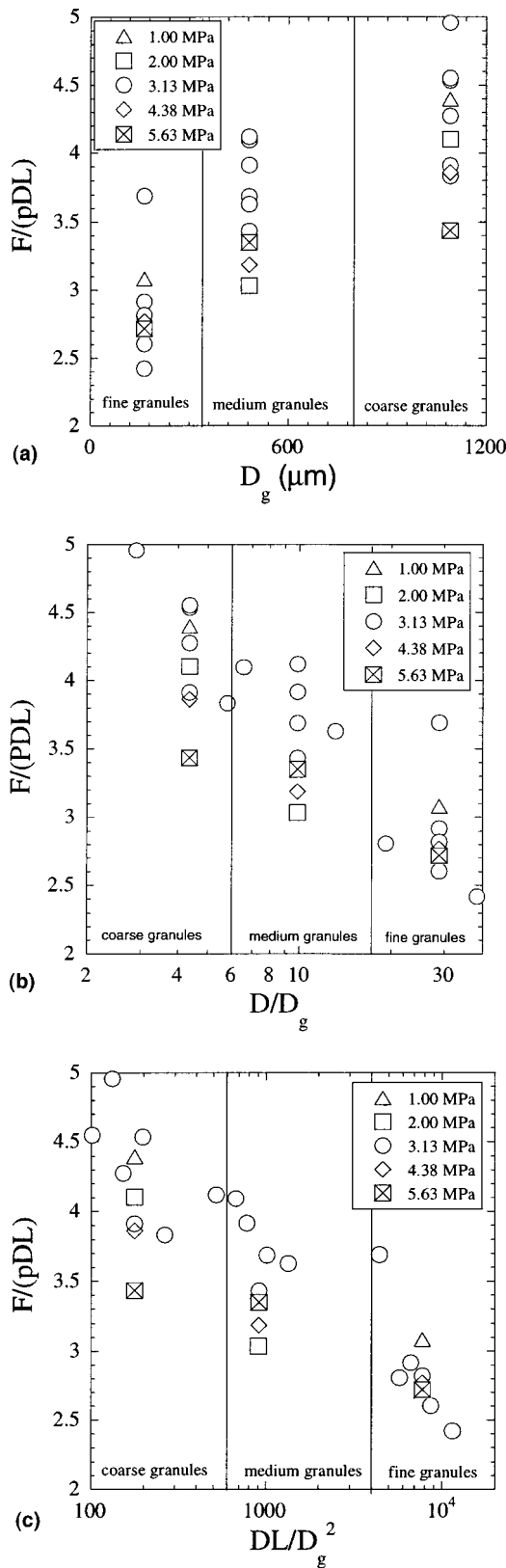
FIG. 9. Normalized drag force as a function of (a) D_g, (b) D/D_g, and (c) $LD/(D_g^2)$. Note that the axes in (b) and (c) are logarithmic.

higher contact density. This trend could be explained through particle rotation effects. As the ratio of D/D_g decreases, the relative curvature of the streamlines increases, and individual particles are subject to increasing rotational kinematics. For perfectly spherical particles, these rotations would be easily accommodated. However, since our particles are irregular and interlocking, particle rotations are possible only through the accommodating motion of neighboring particles or through particle fracture. These resistances to particle rotation lead to the observed increases in drag force. Note that the experiments of Albert *et al.*, which used smooth, spherical particles and no confinement, did not observe any granule size dependence.

It is worth noting that the increase in drag force which we observe for pressurized flow could actually be due to two distinct effects. The application of pressure during the experiment increases intergranular contact forces, which also proportionally increases the sliding resistance of these granules according to Coulombic frictional effects. However, the compression experiments demonstrate that application of pressure also increases the effective density of the granular material, which decreases the free space available for reorganization of the grains during flows. These effects could be tested independently by applying a high compaction pressure, to increase the effective density of the granular bed, then reducing the pressure prior to drag measurements.

The compression results show that the effective granular density increases with an increase in pressure. The results also showed for coarse particles a measurable decrease in compressibility as compression rate increases. The higher compression rates probably reduce the ability of the granular material to reorient and repack individual granules optimally, suggesting that there is a fundamental time scale associated with such processes. No corresponding change in drag behavior was noted for fine particles at different drag velocities. However, since our drag apparatus is only capable of generating relatively low compaction pressures relative to the pressures required to see appreciable velocity effects (6 MPa versus $\sim$30 MPa), such velocity effects may become apparent at higher compaction pressures.

The micrographs indicate that grain fracturing is occurring during drag experiments. However, the development of a steady drag force indicates that the processes of damage and flow are part of a continuous process and do not result in a localized accumulation of fractured granules.

V. CONCLUSIONS

The experimental investigation of drag flow in pressurized granular materials shows that drag flow in confined, pressured granular beds is significantly different from drag flow in unconfined granular materials. Specifically, the drag forces for confined flow are much higher than unconfined flows and scale linearly with compaction pressure. Additionally, the drag force in confined flows is strongly dependent on the granule size. These behaviors could reflect the importance of particle-to-particle contacts or particle-to-cylinder contacts during drag flow. Both these drag results and the

compression results should prove useful for forming constitutive equations for modeling general flows of pressurized, confined granular media. However, further fundamental experiments are required to fully understand the relative importance of fracture, reorganization, deformation, and frictional sliding during such processes.

[1] L. Bocquet, W. Losert, D. Schalk, T. C. Lubensky, and J. P. Gollub, Phys. Rev. E **65**, 011307 (2002).

[2] A. Srivastava and S. Sundaresan, Powder Technol. **129**, 72 (2003).

[3] P. Vainshtein, M. Fichman, M. Shapiro, L. Moldavsky, and C. Gutfinger, Int. J. Multiphase Flow **25**, 1431 (1999).

[4] D. Chehata, R. Zenit, and C. R. Wassgren, Phys. Fluids **15**, 1622 (2003).

[5] G. I. Tardos, S. McNamara, and I. Talu, Powder Technol. **131**, 23 (2003).

[6] J. F. Klausner, D. M. Chen, and R. W. Mei, Powder Technol. **112**, 94 (2000).

[7] G. I. Tardos, M. I. Khan, and D. G. Schaeffer, Phys. Fluids **10**, 335 (1998).

[8] N. Hu and J. F. Molinari, J. Mech. Phys. Solids **52**, 499 (2004).

[9] L. S. Mohan, K. K. Rao, and P. R. Nott, J. Fluid Mech. **457**, 377 (2002).

[10] G. Ovarlez, E. Kolb, and E. Clement, Phys. Rev. E **64**, 060302 (2001).

[11] R. Albert, M. A. Pfeifer, A. L. Barabasi, and P. Schiffer, Phys. Rev. Lett. **82**, 205 (1999).

[12] I. Albert, P. Tegzes, R. Albert, J. G. Sample, A. L. Barabasi, T. Vicsek, B. Kahng, and P. Schiffer, Phys. Rev. E **64**, 031307 (2001).

[13] I. Albert, P. Tegzes, B. Kahng, R. Albert, J. G. Sample, M. Pfeifer, A. L. Barabási, T. Vicsek, and P. Schiffer, Phys. Rev. Lett. **84**, 5122 (2000).

[14] B. Kahng, I. Albert, P. Schiffer, and A. L. Barabasi, Phys. Rev. E **64**, 051303 (2001).

[15] I. Albert, J. G. Sample, A. J. Morss, S. Rajagopalan, A. L. Barabasi, and P. Schiffer, Phys. Rev. E **64**, 061303 (2001).

[16] G. D'Anna, Europhys. Lett. **51**, 293 (2000).

[17] S. Nasuno, A. Kudrolli, and J. P. Gollub, Phys. Rev. Lett. **79**, 949 (1997).

[18] W. A. Gooch, M. S. Burkins, G. Hauver, P. Netherwood, and R. Benck, J. Phys. IV **10**, 583 (2000).

[19] R. Subramanian and S. J. Bless, Int. J. Impact Eng. **17**, 807 (1995).

[20] D. A. Shockey, A. H. Marchand, S. R. Skaggs, G. E. Cort, M. W. Burkett, and R. Parker, Int. J. Impact Eng. **9**, 263 (1990).

[21] E. W. Andrews and K. S. Kim, Mech. Mater. **29**, 161 (1998).

[22] R. Cortes, C. Navarro, M. A. Martinez, J. Rodriguez, and V. Sanchez-Galvez, Int. J. Impact Eng. **12**, 639 (1992).

[23] D. R. Curran, L. Seaman, T. Copper, and D. A. Shockey, Int. J. Impact Eng. **13**, 53 (1993).

[24] T. G. Sitharam, Mech. Mater. **31**, 653 (1999).

[25] A. N. Norris and D. L. Johnson, Trans. ASME, J. Appl. Mech. **64**, 39 (1997).

[26] D. L. Johnson, H. A. Makse, N. Gland, and L. Schwartz, Physica B **279**, 134 (2000).

[27] L. W. Meyer and I. Faber, J. Phys. IV **7**, 565 (1997).

[28] D. H. Zeuch, J. M. Grazier, J. G. Arguello, and K. G. Ewsuk, J. Mater. Sci. **36**, 2911 (2001).

[29] R. W. Klopp and D. A. Shockey, J. Appl. Phys. **70**, 7318 (1991).

[30] C. J. Shih, M. A. Meyer, and V. F. Nesterenko, Acta Mater. **46**, 4037 (1998).

[31] S. C. Cowin, Acta Mech. **20**, 41 (1974).

[32] M. A. Goodman and S. C. Cowin, J. Fluid Mech. **45**, 321 (1971).

[33] W. A. M. Brekelmans, Powder Technol. **62**, 21 (1990).

[34] H. S. Kim, S. T. Oh, and J. S. Lee, J. Am. Ceram. Soc. **85**, 2137 (2002).

[35] S. C. Cowin, Powder Technol. **9**, 61 (1974).

[36] R. M. Nedderman, *Statics and Kinematics of Granular Materials* (Cambridge University Press, Cambridge, England, 1992), p. 84.